Electric Power Systems Research 167 (2019) 94–112

Contents lists available at ScienceDirect

Electric Power Systems Research

journal homepage: www.elsevier.com/locate/epsr

Optimal planning of battery systems for power losses reduction in distribution grids

P. Lazzeroni[a,*], M. Repetto[b]

[a] Fondazione LINKS - Leading Innovation & Knowledge for Society, Via Pier Carlo Boggio, 61, 10138, Torino, Italy
[b] Politecnico di Torino, DENERG - Energy Department "Galileo Ferraris", Corso Duca degli Abruzzi, 24, 10129, Torino, Italy

ARTICLE INFO

Keywords:
MIQCQP
Power losses minimization
Battery management
Battery size and location

ABSTRACT

The minimization of the power losses in the distribution grid is one of the main issue for the Distribution System Operator in order to reduce the management costs of the grid. The recent development of the battery technologies has introduced new possible applications for these systems within the radial distribution grid. In fact, batteries can be opportunely integrated in the grid and managed in order to reduce the power losses, and consequently increasing, for instance, the penetration of the renewable distributed generation and contributing to voltage regulation through reactive power production from battery inverter. In this context, one of the main research interest is the definition of the optimal siting and sizing of the energy storage solutions, considering a battery management capable to reduce network power losses and taking into account battery installation costs.

Since network losses are expressed by means of quadratic function, an approach based on Mixed Integer Quadratically Constrained Quadratic Programming is proposed here to identify possible batteries optimal management strategies capable to minimize the power losses. Evaluation of the grid variables is obtained by the iterative Backward/Forward Sweep method implemented within the formulation of the optimization problem. The reactive power generated by the battery inverter is modeled as well by introducing quadratic constraints in order to further contribute in the network power losses reduction, taking into account the power factor limitation due to the inverter capability curve.

An optimization procedure, called D-XEMS13, based on the formulation of the optimization problem, is implemented within a single loop optimization algorithm in order to identify the best size of the connected BESSs units, capable to maximize the reduction of the power losses in test grids. BESS optimal placement is also identified through a proposed approach based on a nodal sensitivity analysis of the network power losses. Validation of the proposed approach is then obtained by means of a cost/benefit comparison from energy point of view.

Finally, the single loop optimization algorithm is further implemented on two test grids with optimal BESSs sizes and siting, assuming different capability curves for the BESS inverters. The results of simulations with the corresponding benefits are then presented and discussed.

1. Introduction

The power losses represents one of the main issues for the Distribution System Operators (DSOs), since the planning, management and maintenance of a distribution grid are based on the corresponding costs. Consequently, the supply cost offered for the electric power distribution service by the DSOs to the end-user connected to the grid is also affected by the cost related of power losses. Thus a reduction of the power losses represents one of the main goal for DSOs which need to ensure efficient and reliable electricity distribution at affordable price [1]. Contemporarily, the distributed generation also from Renewable Energy Source (RES) is growing in the recent years introducing the need of a possible reconfiguration of the present distribution network (DN) capable to reduce line congestion and to ensure lower power losses with a corresponding increased reliability and efficiency [2].

The development of a Smart Grid (SG) approach by means of the implementation of emerging storage technologies represents a possible solution for the planning and the management of the distribution grid, paving the way for more efficient and reliable grids which could also support an increased penetration of distributed RES [3,4]. Within the SG approach, the introduction and the management of the battery energy storage system (BESS) to reduce the power losses in the

* Corresponding author.
E-mail address: paolo.lazzeroni@polito.it (P. Lazzeroni).

https://doi.org/10.1016/j.epsr.2018.10.027
Received 14 March 2018; Received in revised form 11 July 2018; Accepted 23 October 2018
Available online 02 November 2018
0378-7796/

distribution grid is becoming more attractive in the recent years due to a significative increase of technology performances and a prospected decreasing costs of the BESS installation [5]. This holds particularly true especially for some promising technologies like, for example, lithium-ion batteries with an expected reduction of capital costs of about 30–50% in the next years [6,7]. Moreover, BESSs can be also used to supply further services like, for example, the reduction of peak-shaving effects and the contribution on voltage regulation in SGs configuration with high penetration of RES generation [8]. In addition, BESSs inverter can be also considered as well to produce reactive power for further reducing network power losses and voltage drop along branches of the distribution network [9].

For these reasons a wide literature is presently focused on the different possible modeling and simulation of the optimal management of the BESSs connected to the distribution grid [10]. In particular, some works are based on Mixed Integer Linear Programming (MILP) formulation, where linear approximation both of quadratic constraints and in the evaluation of the power losses are introduced. Alternatively, formulation based on Mixed Integer Non Linear Programming (MINLP) were used to consider the non-linearities of the problem. In all these cases, the integer variables are introduced as binary to consider the charge/discharge operations of the battery which are mutually exclusive.

In [11] and [12] a MILP formulation is used to define optimal BESSs management for peak shaving purpose and for reducing operational costs of DN with RES, respectively: in both cases a linear approximation in the power flows calculation is introduced by the simplified DistFlow model in order to overcome the problem of the non-linearities introduced by the network losses.

In contrast to the linear approximation, a MISOCP formulation is used in [13] to minimize operational cost of DN through optimal management of BESSs, where capability curve of dispatchable Distributed Generation (DG) is considered by means of a two-quadrant characteristics. In this case, the formulation used to describe the steady-state operation of a radial DN involves (real and reactive) power balance equations, where the non-linearities for evaluating the network power losses, introduced by the square of the voltage and the current in the constraints, are replaced by linear variables.

A similar approach for describing steady-state operation of radial DN was used in [14], where a mixed-integer quadratically-constrained programming (MIQCP) model is implemented to solve a planning problem in DN taking into account non-linearities of power losses.. Finally, a multi-objective MISOCP is proposed in [15] to minimize power losses and investment cost for planning the best location and size of BESSs in the DN. In this case, BESS are modeled by including full-inverter for the grid connection of the storage unit to the distribution grid, where the non-linearity of its capability curve is approximated by linear functions. Moreover, steady-state operation of radial DN was still modeled according to the approach discussed in [13].

The approach proposed in this paper is instead based on a Mixed-Integer Quadratically Constrained Quadratic Programming (MIQCQP) formulation to consider the non linearity introduced by the network power losses and the capability curve of the battery inverter. Differently from the previous papers, the steady-state operation of the radial DN is modeled through the Backward/Forward Sweep Method (BFSM) presented in [16]. This approach allows to implement the formulation of the problem with a reduced number of active variables, since it is based on current balance instead of power balance equations as considered in [13–15]. So, the power exchanged between nodes are not considered as variable of the problem, but calculated later in post-processing. The optimization procedure introduced here is an upgraded version of the `D-XEMS13` procedure presented in [17] which was based on a MILP formulation with linear approximation of the steady-state operation for the DN. The proposed upgraded procedure is capable to find both the exact solution of the load flow calculation and the optimal scheduling of BESS for minimizing power losses in radial DN. Consequently, load leveling can be acted taking into account also the reactive power generated by the battery inverter according to its capability curve. The proposed MIQCQP formulation is after included within a single loop optimization algorithm for evaluating the optimal sizing of battery units connected to a test grid.

Furthermore, a methodology based on a sensitivity analysis of power losses is also presented in this paper for identifying the best siting of BESS within radial DN. The single loop optimization procedure is implemented on two test grids to validate the proposed methodology. The proposed methodology is capable to easily identify the best siting for the storage unit without including additional binary variables in the optimization problem as in [15] or without adopting genetic algorithm as, for example, in [9].

Finally, the influence of different power factor limitation (i.e. different capability curves) of battery inverter is presented and discussed to highlight the benefits of reactive power generation for reducing network power losses.

The paper is organized as follows: in Section 2 the problem description, the modeling of steady-state operation of DN and BESS are presented; in Section 3 the MIQCQP formulation is discussed; the methodology to optimally locate BESS and the single loop optimization algorithm for sizing the BESS are exposed in Section 4; two radial test grids are presented in Section 5 as case studies to validate the proposed methodology for finding the BESS siting; the same case studies are then used to identify BESS sizing through the single loop optimization algorithm in Section 6 taking into account capability curve of the battery inverter; conclusion are finally presented in Section 7.

2. Problem description

The DN are nowadays designed and operated in radial configuration. The reasons for this choice can be summarized in:

- radial configuration is the best compromise between technical and economic requirements;
- it connects with the lowest path the MV / LV substations, in order to contain the cost of the network;
- it allows the supplying of the load, during the repair of the fault;
- it ensure the tightness of the lines against short circuits.

Even if there are indications that this scheme could be changed in the future to increase the reliability of the system, see for instance [18], radial power flow is a standard in our days. This hypothesis is thus used in the analysis carried out in this paper. In addition, the application of the Backward/Forward Seep Method (BFSM) [16] is used to evaluate branch current and bus voltage of the electrical network. This method combined to the MIQCQP formulation creates an optimal power-flow tool called `D-XEMS13`, that is described in the next Sections, for finding the optimal management of the BESSs to reduce power losses in radial distribution grid.

2.1. Network description

The present formulation used to modeling the radial DN is based on the one presented in [16]. In this DN representation, the data are known for all line impedances and $\bar{S}_k$ is the sum of the complex power values of loads (positive) and generators (negative) connected to node kth. In the following subsections the basic assumptions, the matrix representation of grid topology, the line current and bus voltage calculations are presented.

2.1.1. Numbering and representation conventions

The topological representation of the radial DN is strictly related to the conventions used to number the buses and the branches of the radial grid. For this reason, the following rules are identified and applied according to ones described in [17,16]:

- radial topology implies that the number of nodes is equal to the number of branches;
- branches are numbered starting from network root, number coincides with arrival node and this notation is unique also in case of multiple branches stemming from one node;
- node 0 or common node is placed on transformer secondary winding. The first branch is the transformer short circuit impedance;
- all quantities are expressed in their physical units.

2.1.2. Topological matrices

The numbering of buses and branches proposed in the previous subsection brings to a suitable grid representation where a reduced incidence matrix A and a path matrix P can be defined according to ones proposed in [16]. The reduced incidence matrix $A \in \mathbb{N}^{n,n}$ (node × branch matrix), without the reference 0 node, is a square matrix due to the radial topology of DN. The first node of a branch (i.e. sending) is identified by -1, while the second branch node (i.e. receiving) is identified by $+1$.

Instead, the path matrix $P \in \mathbb{N}^{n,n}$ (node × branch matrix), defines if the branch kth belongs to the path that links the node jth to root node. With the previous assumption can be easily verified that $-[A]^T[P] = [I]$. The previous notation is equal to the one presented in [16] but for the orientation of branches.

2.1.3. Line current and voltage drop computation

Line currents and bus voltages are then calculated in a iterative way according to the BFSM proposed in [16]. The loads connected to the DN are characterized by constant current at each jth iterations. Under this hypothesis, loads power value $\bar{S}_k$ is independent by the voltage $\bar{U}_k$ of the node where they are connected. So, the nodal current drawn at each bus in a given jth iteration of BFSM is then defined by:

$$\bar{I}_{\mathrm{nk}}^{(j)} = \frac{\bar{S}_k^*}{3\bar{U}_k^{*(j-1)}} \tag{1}$$

where the value of $\bar{U}_k^{(j-1)}$ is the nodal (phase) voltage calculated at the previous iteration j-1. During the iterative process of BFSM, the bus voltages used to evaluate the nodal currents in Eq. (1) are supposed to be equals to $\bar{E}_0$ for all the nodes only at the first iteration.

The corresponding Kirchhoff Current Law at each node can be written for each iteration by using incidence matrix notation as follows:

$$[A]\{\bar{I}_b^{(j)}\} = \{\bar{I}_n^{(j)}\} \tag{2}$$

where RHS array is given by Eq. (1).

Once branch currents are computed by the previous equations, the voltage drop $d\bar{U}_k$ along each kth branch of the grid can be written as follows:

$$d\bar{U}_k^{(j)} = \bar{Z}_k \bar{I}_{\mathrm{bk}}^{(j)} \tag{3}$$

where $\bar{Z}_k$ is the series impedance of the kth branch.

Consequently, the bus voltage in each bus can be then written at each jth iterations, as follows:

$$\{\bar{U}^{(j)}\} = \bar{E}_0 - [P]\{d\bar{U}^{(j)}\} \tag{4}$$

where $\bar{E}_0$ is the known voltage of the root or slack node and $d\bar{U}$ is the vector of the voltage drops along each kth branch.

Finally, the iterative process continues until the following convergence criteria is reached:

$$\left| \frac{\{\bar{U}^{(j)}\} - \{\bar{U}^{(j-1)}\}}{\{\bar{U}^{(j-1)}\}} \right| \leq \epsilon \tag{5}$$

In other words, the iterative process of BFSM is stopped when the relative difference of bus voltages of two consecutive iterations is lower than a ϵ fixed value.

2.2. BESS modeling

The formulation of the BESS model in based on one introduced in [19], where the battery is treated by the passive components convention. Consequently, the power injected into the battery has positive sign, while the power produced by the battery and injected into the grid has negative sign. The energy content of the battery (i.e. its State Of Charge) SOC at a given time instant t_{i+1} is defined by the following linear equations:

$$\mathrm{SOC}(t_{i+1}) = \eta_{\mathrm{sd}}\mathrm{SOC}(t_i) + \left(\eta_c P_{\mathrm{st},c}(t_i) - \frac{P_{\mathrm{st},d}(t_i)}{\eta_d}\right)\Delta t \tag{6}$$

where η_{sd} is the self-discharge efficiency, η_c is the charge efficiency, η_d is the discharge efficiency and $P_{st,c}$ and $P_{st,d}$ are the battery power respectively during charge and discharge phase. The previous quantities are related by inequality constraints in order to limit the power injected into and retrieved from the battery, as follows:

$$0 \leq P_{\mathrm{st},c} \leq \delta_c \frac{\mathrm{SOC}_{\max}}{T_c} \tag{7}$$

$$0 \leq P_{\mathrm{st},d} \leq \delta_d \frac{\mathrm{SOC}_{\max}}{T_d} \tag{8}$$

$$0 \leq \delta_c + \delta_d \leq 1 \tag{9}$$

where SOC_{max} is the storage capacity of the battery, T_c and T_d are the minimum charge and discharge time. Eq. (9) is a logical constraint where δ_c and δ_d are binary variables that compel charge and discharge powers to be different from zero only one at a time.

Moreover, the battery is connected to the network by means of a converter capable to generate real and reactive power on its AC side through its capability curve. This curve represent the inverter operating range in terms of real and reactive power. Thus, both real and reactive power exchanged to the grid through the battery inverter are strictly related to the bus voltage $\bar{U}_k$ where BESS is connected and to the current $\bar{I}_{\mathrm{st}}$ of storage unit, as follows:

$$\bar{S}_{\mathrm{st}} = 3\bar{U}_k\bar{I}_{\mathrm{st}}^* = P_{\mathrm{st}} + jQ_{\mathrm{st}} = (P_{\mathrm{st},c} - P_{\mathrm{st},d}) + jQ_{\mathrm{st}} \tag{10}$$

where the reactive power Q_{st} exchanged to the inverter can assume positive or negative values according to its capability curve. Consequently, in each jth iterations of BFSM, the relationship between the real/reactive power exchanged to the battery and the real/imaginary part of the battery current of a BESS connected to a generic kth node is calculated, as follows:

$$\Re[\bar{U}_k^{(j-1)}]\Re[\bar{I}_{\mathrm{st}}^{(j)}] + \Im[\bar{U}_k^{(j-1)}]\Im[\bar{I}_{\mathrm{st}}^{(j)}] = \frac{P_{\mathrm{st,c}}^{(j)} - P_{\mathrm{st},d}^{(j)}}{3} \tag{11}$$

$$\Im[\bar{U}_k^{(j-1)}]\Re[\bar{I}_{\mathrm{st}}^{(j)}] - \Re[\bar{U}_k^{(j-1)}]\Im[\bar{I}_{\mathrm{st}}^{(j)}] = \frac{Q_{\mathrm{st}}^{(j)}}{3} \tag{12}$$

Eqs. (11) and (12) are linear at each jth iterations, since the voltage at the generic k node are calculated at the previous iteration $j - 1$. So, they are used as known parameters in the MIQCQP formulation.

2.2.1. Capability curve of BESS inverter

As already observed, the BESS unit is connected to the radial distribution grid through inverter which could be potentially controlled by the DSO to operate as four quadrant power converter. The aim is to exchange reactive power from the BESS inverter to compensate the reactive power fluxes of the network and consequently to further reduce the power losses as a power factor correction unit. In fact, as shown in Fig. 1, the capability curve is the ability of the inverter to produce real and reactive power within its operating range represented by the red dashed area. Thus, when the real power is exchanged during charge or discharge phase and if limitation are imposed to the power factor of the energy exchanged to the battery, the reactive power can be

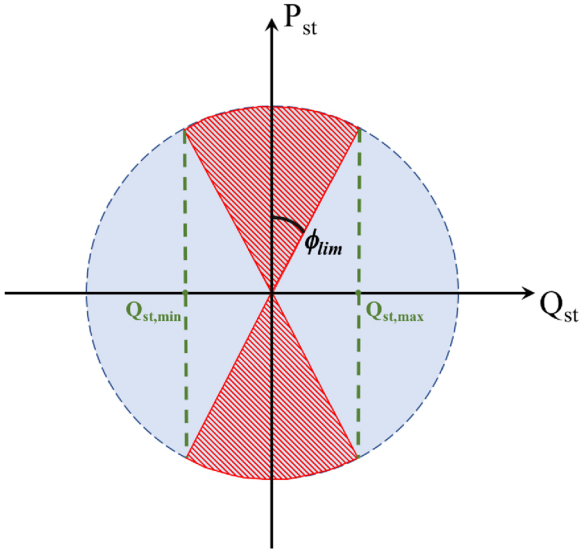

Fig. 1. Capability curve for BESS inverter.

opportunely selected within the red dashed area.

For this reason, additional quadratic constraints are introduced during the charging and discharging phase to limit, through its capability curve, the reactive power that can be generated by the BESS inverter:

$$P_{st,c}^2 + Q_{st}^2 \leq S_{max}^2 \tag{13}$$

$$P_{st,d}^2 + Q_{st}^2 \leq S_{max}^2 \tag{14}$$

Where the reactive power generation is bounded according to the capability curve, as follows:

$$Q_{st,min} \leq Q_{st} \leq Q_{st,max} \tag{15}$$

For the sake of simplicity, the maximum apparent power S_{max} of the inverter is set equal to the maximum real power supplied by the BESS.

Furthermore, if the power factor of the battery inverter is limited by its technical characteristics, the capability curve is limited as well by means of additional linear constraints. In particular, the real and the reactive power generated by the battery inverter can be managed only within the range imposed by the limited power factor $\cos\phi_{lim}$. This range is represented by the red dashed area in Fig. 1. For instance, if $\cos\phi_{lim} = 0$ the inverter can be managed as a four-quadrant inverter, so battery inverter can potentially inject reactive power into the grid even when the real one is not exchanged with the BESS.

The feasible region represented by the red dashed area, is then subdivided in two parts related to charge and discharge phase in order to keep the convexity of the problem. This can be done by introducing two additional variables $Q_{st,c}$ and $Q_{st,d}$, and the following linear constraints:

$$Q_{st,c} - P_{st,c} \tan\phi_{lim} \leq 0 \tag{16}$$

$$Q_{st,c} + P_{st,c} \tan\phi_{lim} \geq 0 \tag{17}$$

$$Q_{st,d} - P_{st,d} \tan\phi_{lim} \leq 0 \tag{18}$$

$$Q_{st,d} + P_{st,d} \tan\phi_{lim} \geq 0 \tag{19}$$

$$Q_{st} = Q_{st,d} + Q_{st,c} \tag{20}$$

These equations ensure that reactive power generated by the battery inverter respects the power factor limitation both during charge and during discharge phase. In particular, $P_{st,c}$ is zero when storage is discharged, so $Q_{st,c}$ is zero as well owing to Eqs. (16) and (17). Vice versa, $P_{st,d}$ is zero when battery is charged, so $Q_{st,d}$ is zero as well owing to Eqs. (18) and (19).

3. Problem formulation

The implementation of the aforementioned linear and quadratic equations is realized within a MIQCQP environment. This need is owing to the following aspects:

- binary (i.e. integer) control variable are introduced to manage charge and discharge phase of the battery
- reactive power supplied by battery inverter is constrained by its capability curves represented through quadratic constraints
- network power losses are calculated through quadratic formulation

The proposed procedure is used to evaluate and minimize the power losses of an active distribution grid with BESS optimal scheduling. Due to the active nature of the network (i.e. the battery could inject power into the grid), the branch currents $\bar{I}_{bk}$ can flow in both directions along each branch. This condition can be taken into account by introducing two auxiliary current variables in order to define a branch current $\bar{I}_{bk}$ that can assume both positive and negative values. Consequently, $\bar{I}_{bk,\,in}$ and $\bar{I}_{bk,\,out}$ are defined for each branch according to the two possible directions of the current. The relationship between the generic branch current $\bar{I}_{bk}$ and the current $\bar{I}_{bk,\,in}$ and $\bar{I}_{bk,\,out}$ is defined by a constraints as follows:

$$\bar{I}_{bk} = \bar{I}_{bk,\,in} - \bar{I}_{bk,\,out} \tag{21}$$

A representation of Eq. (21) is shown in Fig. 2, with the assumption that the positive current is the one entering a node.

Inside MIQCQP formulation of the optimization problem, the complex numbers are split in their real and imaginary parts. Therefore, a separated formulation is necessary for the real part and the imaginary part of all the phasors.

Eqs. (22) and (23) define respectively the real and imaginary part of the branch current. The value of $\Re[\bar{I}_{bk}]$ can assume both positive and negative values, while the values of $\Re[\bar{I}_{bk,\,in}]$ and $\Re[\bar{I}_{bk,\,out}]$ are only positive, according to the convention shown in Fig. 2. The same considerations are valid for the (23).

$$\Re[\bar{I}_{bk}] = \Re[\bar{I}_{bk,\,in}] - \Re[\bar{I}_{bk,\,out}] \tag{22}$$

$$\Im[\bar{I}_{bk}] = \Im[\bar{I}_{bk,\,in}] - \Im[\bar{I}_{bk,\,out}] \tag{23}$$

In previous equations the two contributes to the current component, as for instance $\Re[\bar{I}_{bk}]$ are constrained to be positive by the addition to the LP of two inequality constraints:

$$\Re[\bar{I}_{bk,\,in}] > 0, \quad \Re[\bar{I}_{bk,\,out}] > 0 \tag{24}$$

Finally, the considerations described here for the branch current $\bar{I}_{bk}$ are also used for the storage current $\bar{I}_{st}$.

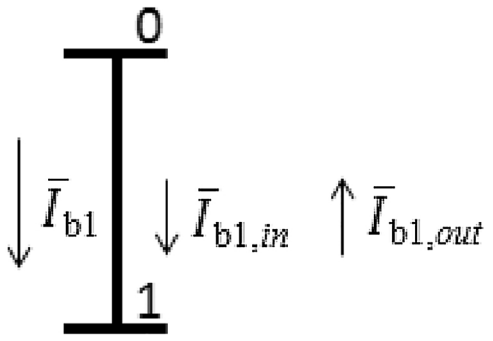

Fig. 2. Branch currents phasors defined by means of two auxiliary variables $\bar{I}_{bk,\,in}$ and $\bar{I}_{bk,\,out}$.

3.1. Definition of the objective function

The linear treatment of the currents inside the network by means of phasors allows to compute the real and imaginary part of all the network variables. On the other hand, the computation of DN power losses requires the evaluation of the square of absolute value of the currents. This operation introduces a further non linearity. The problem can be tackled by using a quadratic programming by means of a MIQCQP formulation.

In particular, the magnitude squared value is calculated as the sum of the squared values of real and imaginary part of the current phasor $\bar{I}_{bk}$ (see Eq. (25)).

$$|\bar{I}_{bk}|^2 = \Re[\bar{I}_{bk}]^2 + \Im[\bar{I}_{bk}]^2 \tag{25}$$

Replacing Eq. (22) and Eq. (23) in the RHS elements of Eq. (25) we can find two types of non linearity.

$$\Re[\bar{I}_{bk}]^2 = \Re[\bar{I}_{bk,in}]^2 + \Re[\bar{I}_{bk,out}]^2 - 2(\Re[\bar{I}_{bk,in}]\cdot\Re[\bar{I}_{bk,out}]) \tag{26}$$

$$\Im[\bar{I}_{bk}]^2 = \Im[\bar{I}_{bk,in}]^2 + \Im[\bar{I}_{bk,out}]^2 - 2(\Im[\bar{I}_{bk,in}]\cdot\Im[\bar{I}_{bk,out}]) \tag{27}$$

The non linearity resulting from the double product of the two auxiliary variables in Eqs. (26) and (27) is set equal to zero in order to force mutual exclusion of *in* and *out* variables. Consequently, one of the two variables (*in* or *out*) will be equal to zero in the optimal solution, as stated by constraints defined in Eqs. (22), (23) and (24).

Under these hypotheses, the objective function of the optimization procedure is the evaluation of the power losses, within a scheduling period, along all the branches of the radial DN, which are calculated as follows:

$$\begin{aligned} P_{loss} &= \sum_{i=1}^{N}\left(\sum_{k=1}^{n} 3R_k\,|\bar{I}_{bk}(t_i)|^2\right) \\ &= \sum_{i=1}^{N}\left(\sum_{k=1}^{n} 3R_k\left(\Re[\bar{I}_{bk}(t_i)]^2 + \Im[\bar{I}_{bk}(t_i)]^2\right)\right) \\ &= \sum_{i=1}^{N}\left(\sum_{k=1}^{n} 3R_k\left(\Re[\bar{I}_{bk,in}(t_i)]^2 + \Re[\bar{I}_{bk,out}(t_i)]^2 + \Im[\bar{I}_{bk,in}(t_i)]^2\right.\right. \\ &\quad \left.\left. + \Im[\bar{I}_{bk,out}(t_i)]^2\right)\right) \end{aligned} \tag{28}$$

where R_k is the series resistance of the kth branch, N is the number of the time intervals in which the scheduling period is discretized and n is the number of the branches.

The minimization of the power losses P_{loss} can be performed, at each jth iterations of BFSM, by implementing the aforementioned equations under a standard MIQCQP formulation [20], which is defined as follows:

$$\begin{aligned} &\min z \quad = \tfrac{1}{2}x^T\mathrm{R}x + c^Tx \\ &\text{s. t.} \\ &\qquad A_1x \le b_1 \\ &x^TA_2x + \quad c_2^Tx \le b_2 \end{aligned} \tag{29}$$

However, the objective function in Eq. (28) has only quadratic terms as well as the quadratic constraints introduced in Eq. (13) and (14), so the vectors c and c_2 are formed by zero elements. Moreover, the R matrix is diagonal, since the double product of the two auxiliary variables is forced to be zero in Eqs. (26) and (27).

3.2. MIQCQP optimization procedure

The MIQCQP formulation presented in the previous sections has been implemented within an optimization procedure called `D-XEMS13` which is developed inside the MATLAB computational environment. The workflow of the procedure is shown in Fig. 3 and it can be substantially summarized in three steps.

A first step where input data concerning the topology of the radial DN, the branches characteristics (i.e. series impedance, length) and load profiles (i.e. real and reactive power profiles) are acquired. In particular, the network topology is easily created in NEPLAN environment [21], which is a commercial software for load-flow calculation, and then exported to `D-XEMS13`.

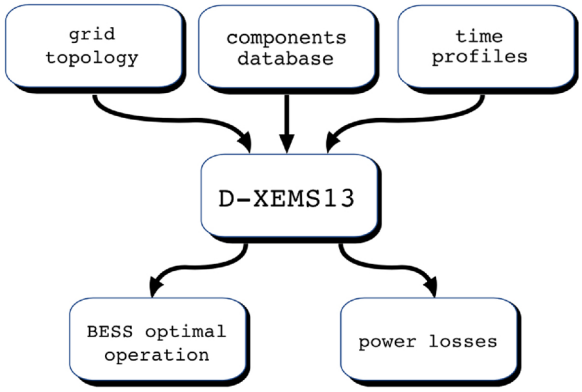

Fig. 3. Workflow of the `D-XEMS13` procedure.

In the second step, the input data are converted into MIQCQP formulation through the `D-XEMS13` procedure under Matlab environment, so that the matrix representation is used as input for the solver integrated within the optimization procedure. In the last step, the results of the optimization (i.e., the scheduling of BESSs, the value of the objective function, branch current and bus voltage) are retrieved and stored for the post-processing analysis.

However, since the optimal operation of BESS has to be found, the optimization procedure needs also to be set over a scheduling period before the first step of the workflow. Even if theoretically the procedure could also work over a week time horizon, the scheduling period is usually set on daily basis since this is the standard discretization based on hourly time intervals. This assumption is capable to reduce both the complexity and the computational time for the solver used inside the optimization procedure.

4. BESS siting and sizing

The optimization procedure described in Section 3.2 can be adopted to manage the SOC of the BESSs connected to a radial distribution grid in order to reduce and minimize line power losses. Ideally, storage units of any size could be placed in all the busbars of a given grid, but best siting and sizing of the batteries needs to be carefully identified to maximize the power losses reduction and contain investment costs.

4.1. BESS siting through sensitivity analysis

The installation of batteries should be avoided in all those nodes with a negligible impact in power losses reduction, both from economic and energy point of view. Otherwise, batteries located in irrelevant busbars could only marginally contribute to power losses reduction and installation costs could raise. In practice, the BESS placement should be optimally performed by adding the BESS units only in all those nodes with higher sensitivity to power losses in order to improve the power losses reduction and saving costs. These nodes can be identified by means of a sensitivity analysis of the power losses.

The methodology consists in the addition of a constant load (i.e. a load with a flat power profile) in a given kth node of the network. After, the corresponding daily power losses $E_{loss,k}$ are calculated for the new grid configuration and subsequently compared to ones obtained in the reference configuration (i.e. the losses calculated for the benchmark DN without loads addition). Then, an indicator is defined in order to measure the sensitivity to power losses of a given kth busbar, as follows:

$$\sigma_{loss,k} = \frac{E_{loss,k} - E^*_{loss}}{E^*_{loss}}100 = \frac{\Delta E_{loss,k}}{E^*_{loss}}100 \tag{30}$$

These procedure was automatically repeated in the NEPLAN

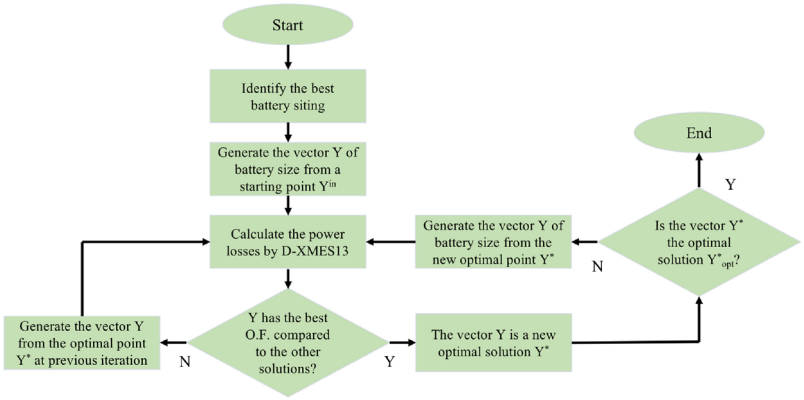

Fig. 4. Workflow of the single loop optimization procedure.

environment for each busbars of the benchmark DN by means of the Neplan Programming Languages [21]. The result is a sorted list in descending order of sensitivity. This list is then used to identify which nodes have to be considered for BESS siting. Finally, the procedure was also tested by changing the rated power and the power factor of the constant loads profile added at each nodes. The resulting sorted lists ensured consistency to the proposed approach, since sensitivity order of the nodes remains unchanged.

4.2. A single loop optimization for sizing BESS

The sizing of the BESS unit connected to the distribution grid is obtained by a single loop optimization algorithm. The approach proposed in this paper uses Pattern Search (PS) [22] as outer loop to evaluate the BESS optimal size minimizing the network power losses calculated by means of MIQCQP. In practice, size of batteries (i.e. SOC_{max} of Eqs. (7) and (8)) connected to a busbar are changed according to the PS method, while power losses are calculated by means of MIQCQP optimization. In this way, the optimal management of the BESSs minimizing power losses is also ensured in each PS iterations.

The proposed algorithm is illustrated in Fig. 4. First of all, the possible placement of batteries is identified in the DN. Secondly, a vector $Y = [SOC_{max,1}, SOC_{max,2}, \ldots, SOC_{max,n}]$ is generated with length equal to the number of busbar where batteries will be placed. Each elements of Y represent the size of the batteries connected to a given node. Beginning from an arbitrary BESS sizes (e.g. $SOC_{max,1} = SOC_{max,2} = \ldots = SOC_{max,n} = 0$), the algorithm explores the solutions space around the starting point by evaluating the objective function (i.e. the power losses through MIQCQP optimization) in a near solution with changed batteries size according to PS procedure. If the near solution has an improved objective function (i.e. the power losses decreases), the point is selected as new optimal solution Y^*, so that the search for optimum continues from this new point. Instead, if the near solution has a worse objective function, the search for optimum restart from the previous point.

PS stops when no improvements of the objective function, within a given tolerance, is found in the solutions space. Under the hypothesis of convex objective function, the optimal solution found Y^*_{opt} represents the best sizes of the storage units connected to the grid capable to improve the minimization of the power losses in the DN.

5. Case studies

The proposed optimization procedure was developed for radial DN, so it was implemented and tested on two different test grids: the CIGRÉ medium voltage (MV) radial distribution grid [23] and the radial distribution grid presented in [9] without renewable generation. The former is the European CIGRÉ benchmark for MV distribution network widely used in literature, where shunt parameters for lines and transformers are not considered by default. The latter is a MV distribution line presented in [9] where shunt parameters for lines and transformer are neglected and renewable generation is not considered. MV distribution lines with shunt admittance could be potentially simulated by modifying the right hand side of Eq. (1) for including the contribution of these parameters to the evaluation of the nodal current drawn at each busbar. However, for the sake of simplicity and without lack of generality, simplified test grids without shunt elements were used here.

5.1. Case study A

This case study is a 14-bus grid connected to the high voltage (HV) sub-transmission system through two HV/MV transformers (see Fig. 5).

Due to the characteristics of the `D-XEMS13` procedure, each HV/MV transformer is converted in an equivalent line, where the corresponding series impedance is equal to one of the equivalent circuit of the transformer referred to secondary winding, so that the grid can be considered as directly connected to an MV node. The data for the transformers of the case study A are shown in A.4. Data of all branches of the grid are instead summarized in Table A.5, while data of load connected to the DN are summarized in Table A.6. In particular, the loads connected to this test grid refer to residential and industrial end-users. Since the optimization procedure operates on scheduling period typically equal to one day, daily load profiles for residential and industrial customers were defined for each end-users, according to the normalized load profiles for real and reactive power presented in [24] and shown in Figs. 6 and 7 . Furthermore, three switches $S1$, $S2$ and $S3$ are placed within the case study in order to generate different possible configurations of the benchmark DN. However, since `D-XEMS13` procedure can operate only for radial distribution grid, the three switches are set to open in the case study.

The BESSs considered in the case study is based on the Lithium-Ion technology, which presently represents one of the best promising technologies with higher energy density, higher roundtrip efficiency and relatively high number of charge/discharge cycles even at higher depth of discharge (DOD). In particular, as shown in Table 1, the roundtrip efficiency is considered approximatively equal to 95% [25], while the DOD is assumed equal to 90%, so that the minimum SOC for the batteries is considered equal to 10% of the maximum storage capacity as assumed in [24]. Moreover, self-discharge η_{sd} is also take into account by considering a 3%/month as reference value for lithium-ion technologies [25].

Finally, it is noticeable that the test grid for the case study A is not provided with distributed generation, so the analysis are focused only either on load shifting or on peak sheaving operation of the storage unit located in the busbars.

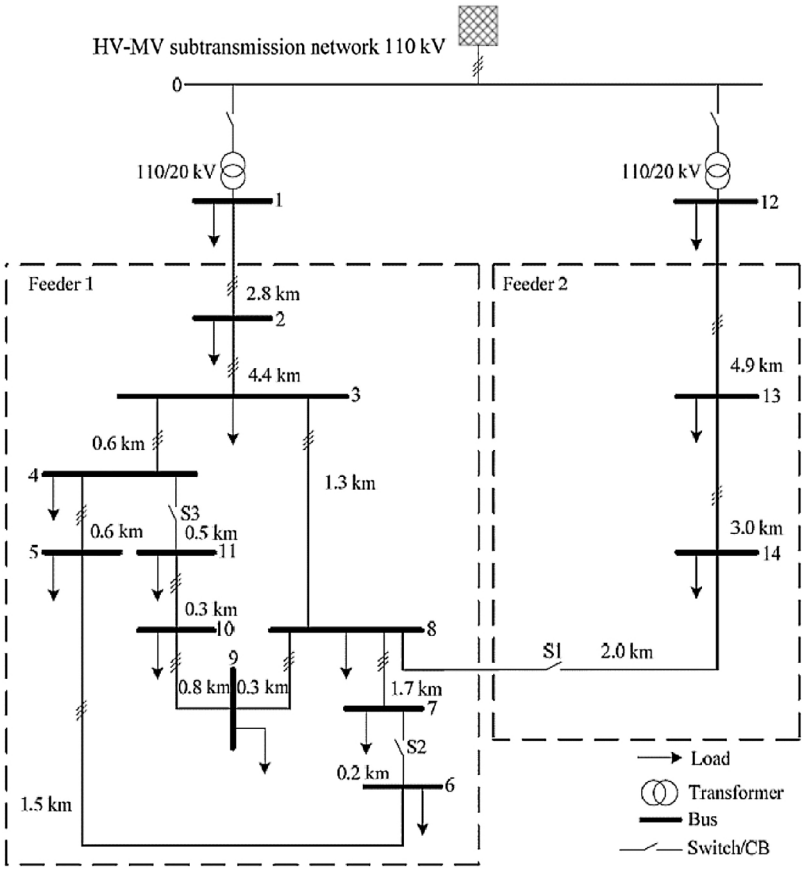

Fig. 5. CIGRÉ European MV distribution network benchmark (case study A).

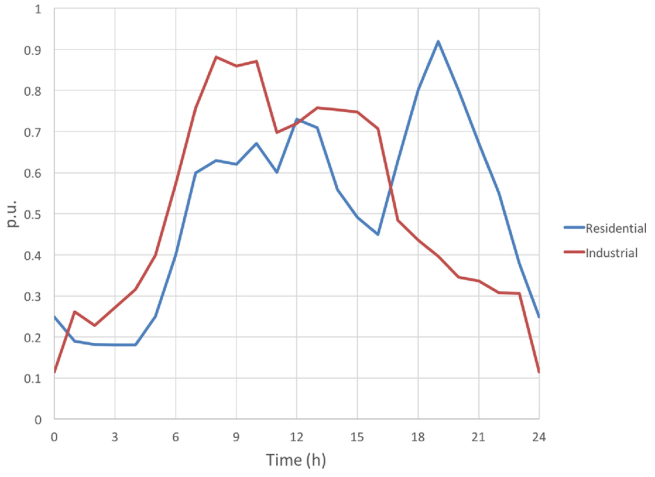

Fig. 6. Normalized real power load profiles.

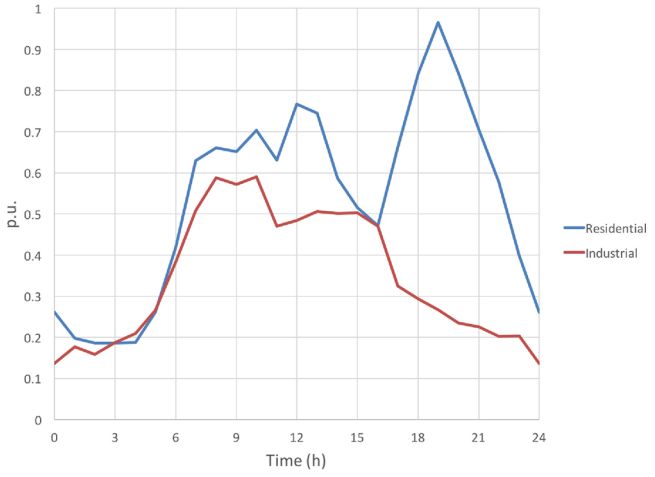

Fig. 7. Normalized reactive power load profiles.

5.2. Case study B

The second case study is instead a 17-bus grid connected to the high voltage (HV) sub-transmission system through a single HV/MV transformers (see Fig. 8).

Similarly to the first case study, the HV/MV transformer is converted into an equivalent line between node 1 and 2 to be compliant to the `D-XEMS13` procedure. Data for the transformer are shown in A.7 . Data of all branches of the grid are instead summarized in Table A.7, while data of load connected to the DN are summarized in Table A.8. Since the optimization procedure operates on scheduling period of one day on hour basis, a daily load profile was also defined in this second case study for each end-users, according to the normalized load profile for real and reactive power presented in [9] and shown in Fig. 9.

Table 1
Technical characteristics of BESS used in the case study A and B

η_{rt}	DOD	η_{sd}	Tc, Td
(%)	(%)	(%/month)	(hour)
95	90	3	1

Finally, the BESSs considered in the case study is still based on the Lithium-Ion technology as already presented in Table 1 for the previous test grid.

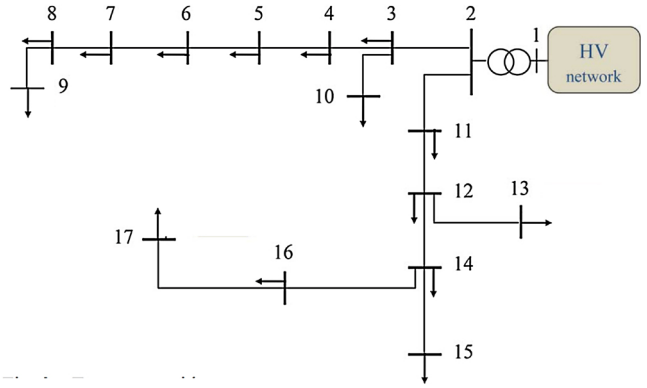

Fig. 8. MV distribution network benchmark for the case study B.

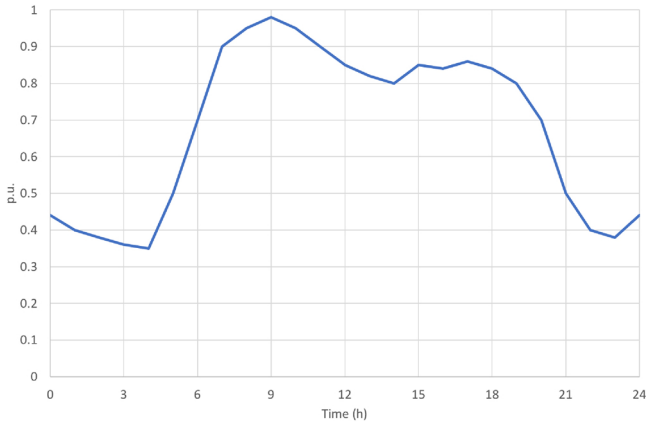

Fig. 9. Normalized real power load profiles.

5.3. Identification of BESS siting and validation

5.3.1. Case study A

The BESS siting for the case study A of Fig. 5 was defined according to the sensitivity analysis presented in Section 4.1. The parameter $\sigma_{loss,k}$ of Eq. (30) was calculated for the test grid by alternatively adding at each busbars loads with flat profiles, but different rated powers and power factors. As pointed out in Section 4.1, the sensitivity order (i.e. the order of the list of nodes sorted by sensitivity) remained unchanged even thought the added flat loads have different rated powers and power factors. An example of the results for the sensitivity analysis is summarized in Table 2 where a constant rated power profile of 500kW with unitary power factor is added alternatively at each busbars. Table 2 highlights that the more sensitive nodes are the first nine, so that contribution to the reduction of daily power losses from nodes 2, 14, 13, 1, 12 could be potentially neglected.

The result exposed in Table 2 was validated by the implementation of the single loop optimization algorithm in the test grid of Fig. 5. The validation was performed by analyzing the results of the single loop optimization for 14 different configurations. These are generated by the addition of a storage unit in each nodes with decreased sensitivity, following the order presented in Table 2. In this way, the configurations were created starting from the first one with only a battery connected to node 11, up to the last one where a battery is connected to each busbars of the grid. For the sake of simplicity, the validation was performed

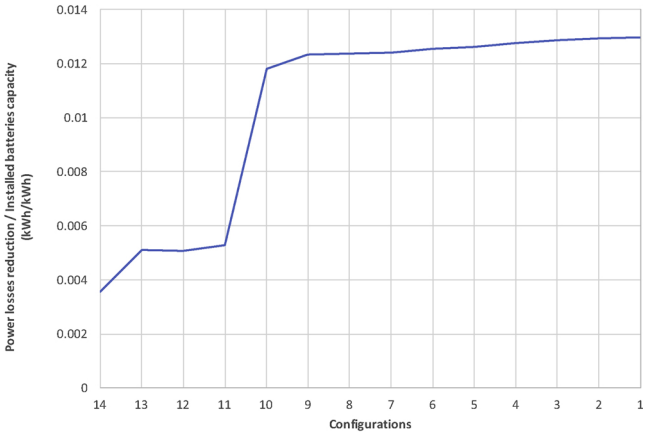

Fig. 10. Trend of the ratio between daily power losses reduction and installed storage capacity for each configurations in case study A.

with power factor of battery inverter set to 1 (i.e. $\cos\phi_{lim} = 1$). The maximum capacity of the storage units was instead leaved unbounded, since the single loop procedure is used here for planning purpose and the feasibility of the optimum search needs to be reached in each configurations.

The power losses reduction and the overall installed battery capacity was calculated for each configurations through the single loop optimization algorithm. Later, the ratio between power losses reduction and installed storage capacity was calculated as well. This ratio represents the power losses reduction potentially achievable from each kWh of installed batteries capacity. It is noticeable that an increasing ratio correspond to a power losses reduction obtained with reduced installed batteries capacity. Vice versa, a decreasing ratio highlights power losses reduction with an increased installed storage capacity. So, higher ratio should be preferred instead of lower one, both form the energy and economic point of view. In fact, the maximum power losses reduction should be ideally reached by minimum installed batteries capacity.

Fig. 10 shows the trend of this ratio for the different configurations. The curve is substantially constant from configuration 1 to 9, but it decreases after the ”knee” at configuration 9. This means that the BESS effect can be potentially maximized from energy and economic point of view in configuration 9 where batteries are connected to the most sensitive nodes in Table 2 (i.e. the first nine of the list). Other configurations have a marginal power losses reduction that is lower than the marginal increase of installed battery capacity. In other words, configurations from 10 to 14 show a power losses reduction which correspond to a significant increase of installed battery capacity. This effect is due to the lower sensitivity impact in power losses reduction of the node 2, 14, 13, 1 and 12, confirming the sensitivity approach proposed here to identify the BESS siting.

5.3.2. Case study B

A similar evaluation was also defined for the case study B. In particular, the sensitivity analysis proposed in the Section 4.1 was also applied for the test grid of Fig. 8. Again, the parameter $\sigma_{loss,k}$ of Eq. (30) was calculated for this test grid by alternatively adding at each busbars loads with flat profiles. The results for the sensitivity analysis for the case study B is summarized in Table 3 where a constant rated power profile of 500kW with unitary power factor is added alternatively at each busbars, excluding the slack node (i.e. node 1 for the case study B).

Table 2
Example of busbar sensitivity to power losses for the case study A

Busbar	11	10	7	9	8	6	5	4	3	2	14	13	1	12
$\sigma_{loss,k}$ **(%)**	25.7	25.6	25.5	24.9	24.4	23.9	23.1	22.6	21.9	8.8	8.0	5.7	0.7	0.6

Table 3
Example of busbar sensitivity to power losses for the case study B

Busbar	17	16	15	14	9	13	12	8	7	6	11	5	4	10	3	2
$\sigma_{loss,k}$ **(%)**	17.9	17.3	14.7	14.6	11.2	10.7	9.6	8.9	7.8	7.5	6.5	5.4	4.5	3.3	2.8	1.5

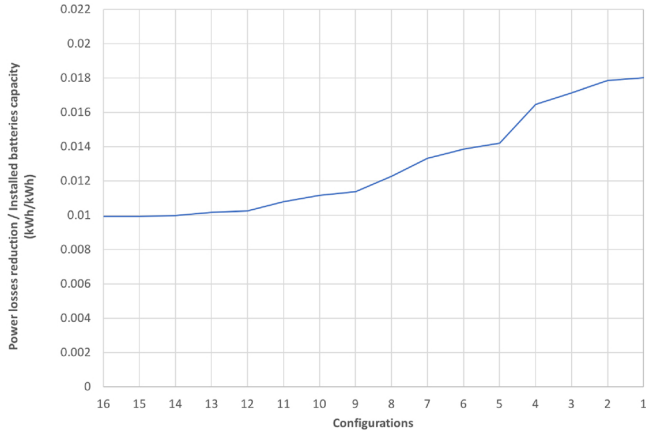

Fig. 11. Trend of the ratio between daily power losses reduction and installed storage capacity for each configurations in case study B.

Differently from the case A, the sensitivity of the busbars decreases more softly in this test grid. However, Table 3 highlights that the more sensitive nodes are expected to be the first two of the list (i.e. nodes 17 and 16), since the marginal reduction of the sensitivity for the other busbars is significant. Thus, the contribution to the reduction of the daily power losses from the other 15 nodes can be potentially neglected.

The result exposed in Table 3 was then validated by the implementation of the single loop optimization algorithm in 16 different configurations of the test grid of Fig. 8. As already explained for the case study A, the configurations are generated by the addition of a storage unit in each nodes with decreased sensitivity, following the order presented in the list of Table 3. In this way, the configurations were created starting from the first one with only a battery connected to node 17, up to the last one where a battery is connected to each busbars of the grid (slack node excluded). The validation was performed with power factor of battery inverter set to 1 (i.e. $\cos\phi_{lim} = 1$). Again, the maximum capacity of the storage units was instead leaved unbounded, as already observed in case study A, since the single loop procedure is used here for planning purpose and the feasibility of the optimum search needs to be reached in each configurations.

After, the ratio between power losses reduction and installed storage capacity was calculated as well. Fig. 11 shows the trend of this ratio for the different configurations of case study B. The curve is substantially constant only for the first two configurations where BESS are installed in the nodes 16 and 17, but it decreases just after the ”knee” at configuration 2. This means that the BESS effect can be potentially maximized from energy and economic point of view in configuration 2 and the other configurations have a marginal power losses reduction that is lower than the marginal increase of installed battery capacity. In other words, configurations from 3 to 16 show a power losses reduction which correspond to a significant increase of installed battery capacity. This effect is due to the lower sensitivity impact in power losses reduction, confirming the sensitivity approach proposed here to identify the BESS siting.

6. Simulations and results

The single loop optimization algorithm presented in the previous sections was used to point out the effect of the battery management to reduce power losses, taking into account the influence of the power factor limitation of the battery inverter. As already observed in Section 5.3.1, the sensitivity analysis highlights that only the more sensitive nodes are relevant to contribute in power losses reduction (i.e. the first nine nodes of the test grid A in Table 2 and the first two of the test grid B in Table 3). Consequently, the single loop optimization is evaluated assuming storage unit connected only in these busbars. The simulations were performed on an Intel Core i7 processor with 3.1 GHz and 16GB of RAM by using the MATLAB interface for GUROBI optimizer [26]. As a general remark, the convergence to the solution of these case studies follows the criteria presented in [16]: higher the load of the grid, higher the number of iterations to reach the convergence and thus the optimal solution.

The test grids presented in Section 5 were simulated with the single loop optimization algorithm capable to evaluate the storage sizes considering different $\cos\phi_{lim}$ for the battery inverter in order to minimize network power losses. As already observed, the test grids are not provided with distributed generation, so the implementation of single loop

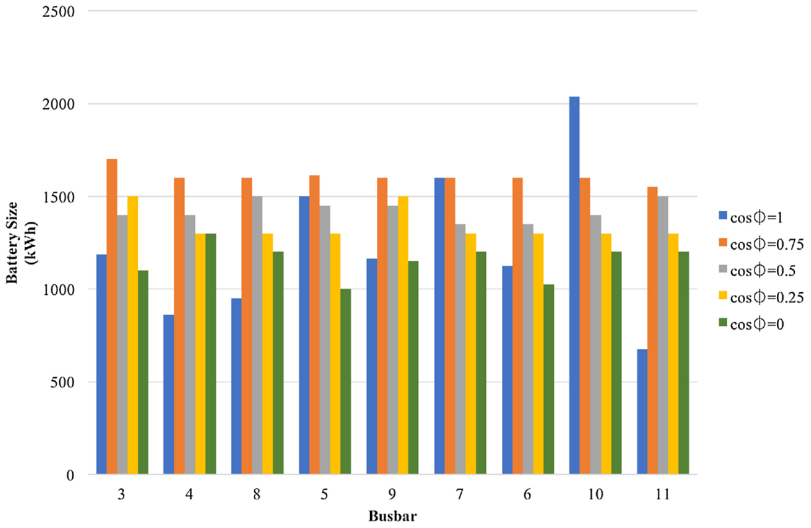

Fig. 12. Batteries size calculated by single loop optimization with different power factor limitation of the battery inverter in case study A.

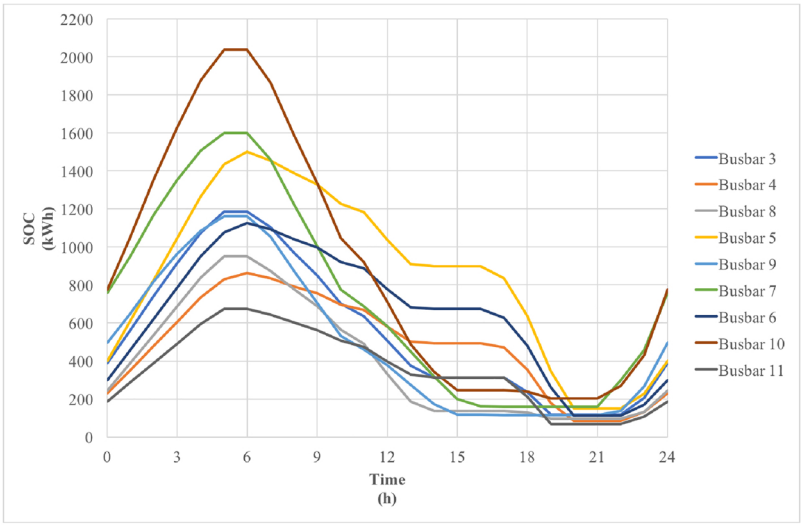

(a)

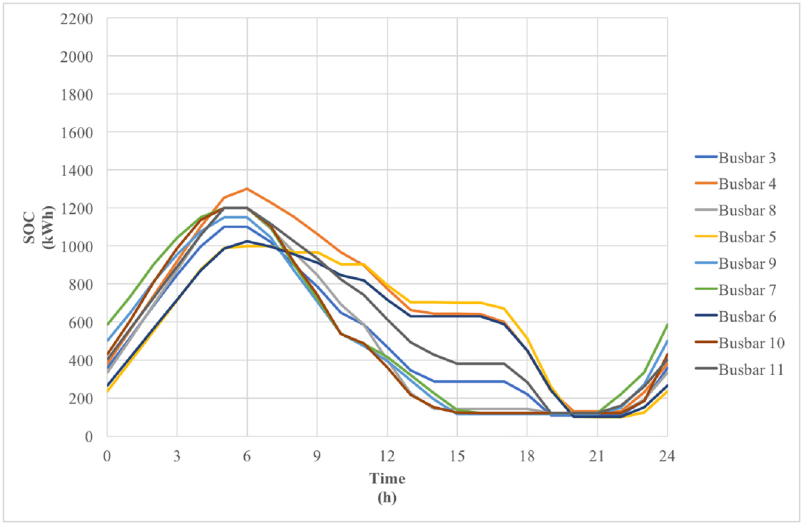

(b)

Fig. 13. State Of Charge for batteries connected to the most sensitive busbars of case study A: (a) storage with $\cos\phi_{lim}=1$; (b) storage with $\cos\phi_{lim}=0$.

optimization is focused only either on load shifting or on peak sheaving operation of the storage unit located in the busbars. Generally, the first expected contribution of the battery is a variation of its *SOC* (i.e. its energy content) which corresponds to a variation of the real power exchanged to the grid. Secondly, the battery inverter contributes to the reactive power generation in order to compensate the reactive power flux along the branches or the lack of power factor. Main results of the different case studies are presented in the following sections.

6.1. Case study A

Fig. 12 summarizes the results of the simulation where the batteries size obtained for different power factor limitation of battery inverter are presented. In general, when the power factor is strongly limited (e.g. $\cos\phi_{lim}=0.75$) the storage size increases, if compared to the configuration with $\cos\phi_{lim}=1$, since higher reactive power can be produced only when higher real one is exchanged to the battery, as can be observed in the capability curve of Fig. 1. Instead, battery inverter without power factor limitation (i.e. $\cos\phi_{lim}=0$) has reduced size, since reactive power can be produced even when real one is not exchanged to the storage unit.

Further results are instead presented in Fig. 13a and b, where the SOC variations due to the management of the battery through the `D-XEMS13` procedure is shown. It is noticeable that the minimum SOC equal to 10% of the battery capacity is substantially always reached in the batteries when the peak load for residential end-users is reached as well (see Figs. 6 and 7). Vice versa, the maximum SOC corresponds to the minimum of the load demand. This is due to the trend of the load profiles for residential end-users, which significantly influence the results in the test grid if compared to industrial one (see Table A.6). In practice, the load shifting is obtained by storing energy during lower users demand and consequently released during the peak demand as expected.

The bus voltages are also evaluated and monitored in the simulations performed by the single loop optimization algorithm in order to verify the limits imposed by the European standard EN50160 [27] for the distribution grid. Fig. 14a highlights that without storage units connected to the grid, the busbar voltages are compliant to the standard requirement since the voltage drops on busbars are lower than 5.95% of the rated value (i.e. 20 kV). Fig. 14b shows that the introduction of

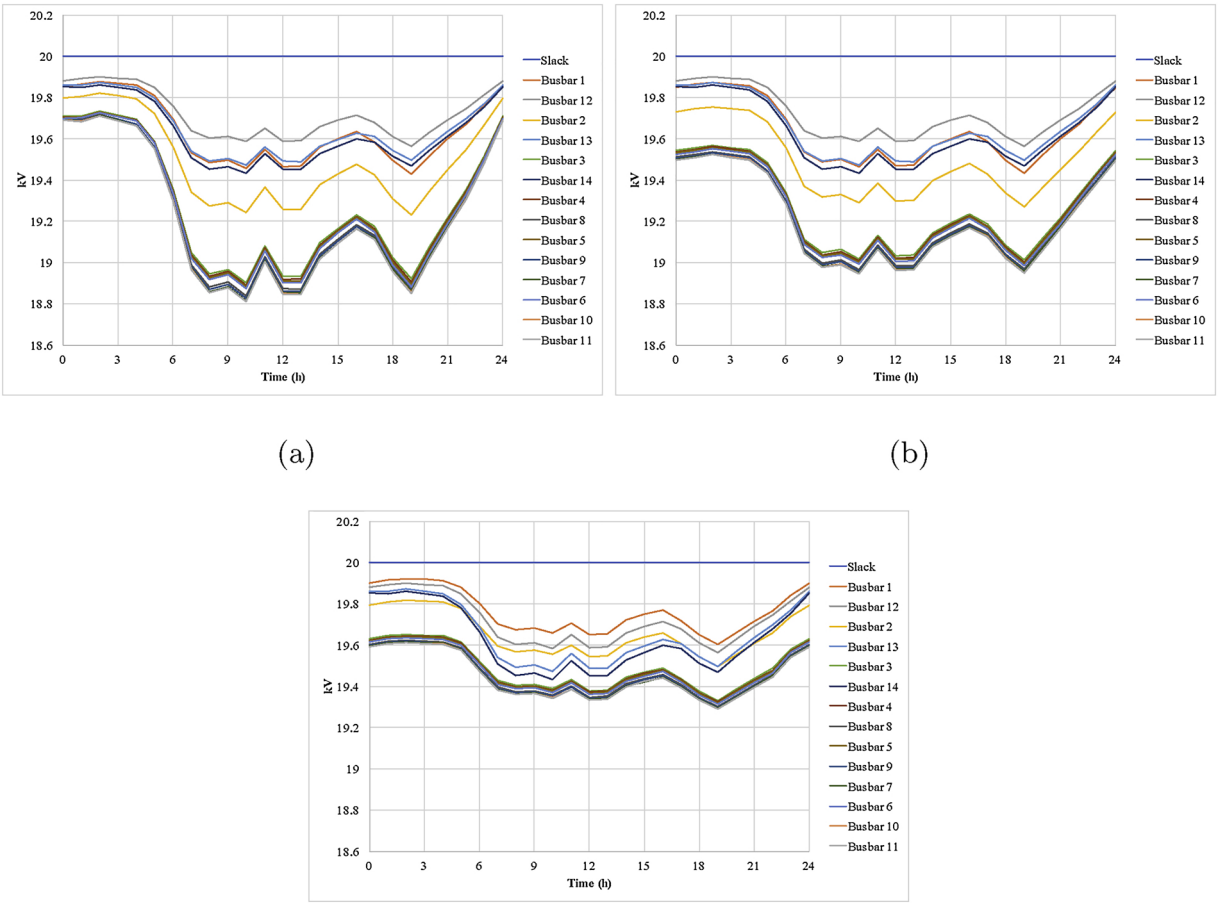

Fig. 14. Busbar voltage profiles of case study A: (a) w/o storage; (b) storage with $\cos\phi_{lim}=1$; (c) storage with $\cos\phi_{lim}=0$.

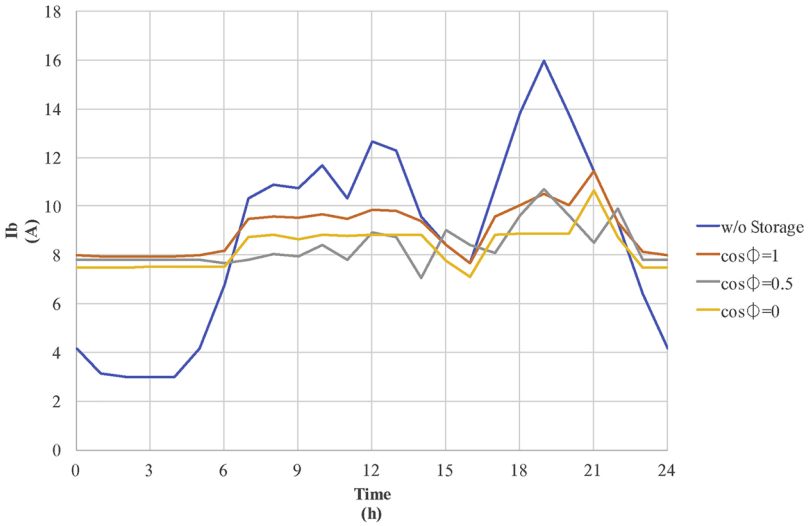

Fig. 15. Line current calculated on branch 6 of case study A with different power factor limitation of the battery inverter.

batteries without reactive power generation reduce the voltage drops. In particular, busbar voltage drops are lower than 5.28% of the reference value. Finally, Fig. 14c shows that the introduction of batteries with production of reactive power by battery inverter, further reduce the voltage drops in busbars down to 3.55%. As a consequence, the placement of storage units significantly contributes to reduce voltage drops along branches ensuring compliance to the European standard.

Moreover, another relevant effect due to the integration of storage unit in the distribution network is observed. In fact, the flattening of the branches current profiles is also reached, since this configuration represents a minimum for the power losses. Figs. 15 and 16 highlight the trend of the RMS value of the current for branch 6 and 9 where

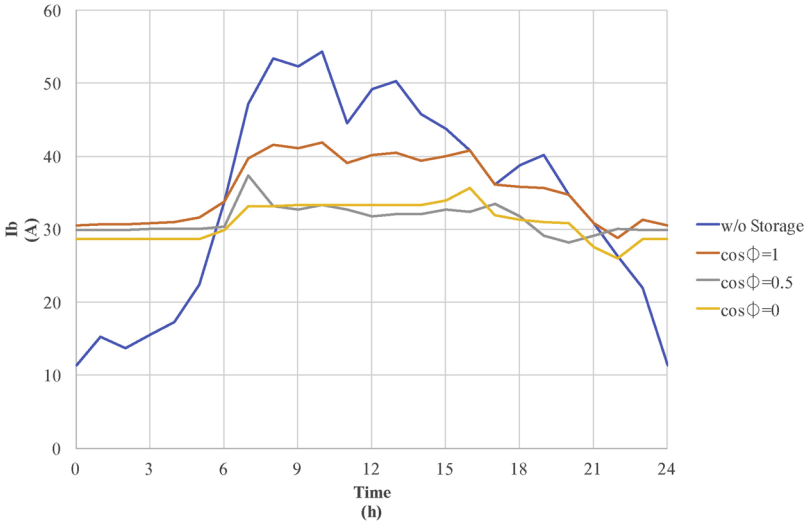

Fig. 16. Line current calculated on branch 9 of case study A with different power factor limitation of the battery inverter.

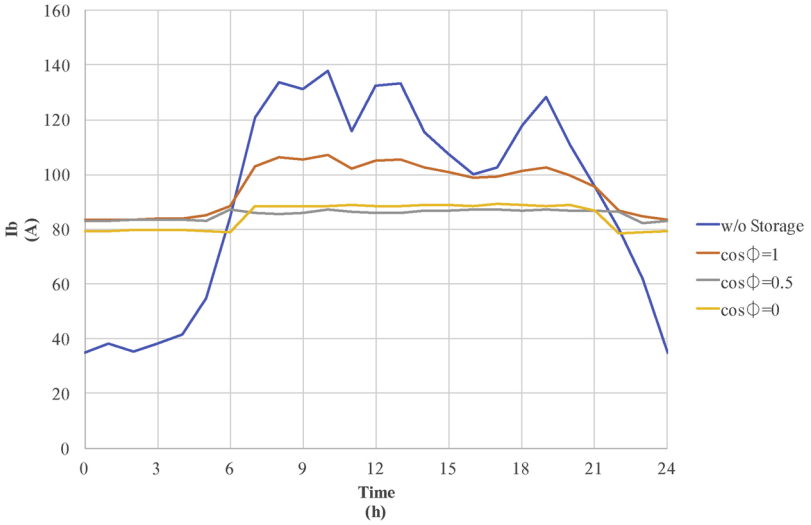

Fig. 17. Line current calculated on branch 3 of case study A with different power factor limitation of the battery inverter.

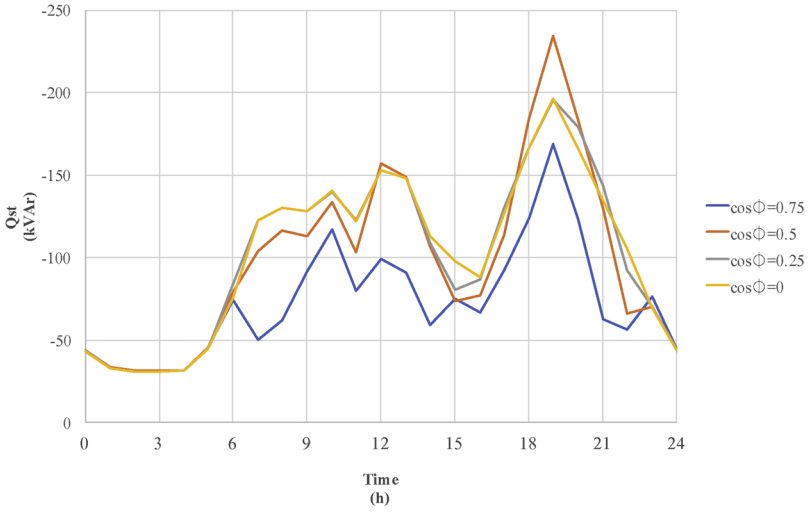

Fig. 18. Reactive power produced by battery inverter connected to busbar 6 of case study A with different power factor limitation.

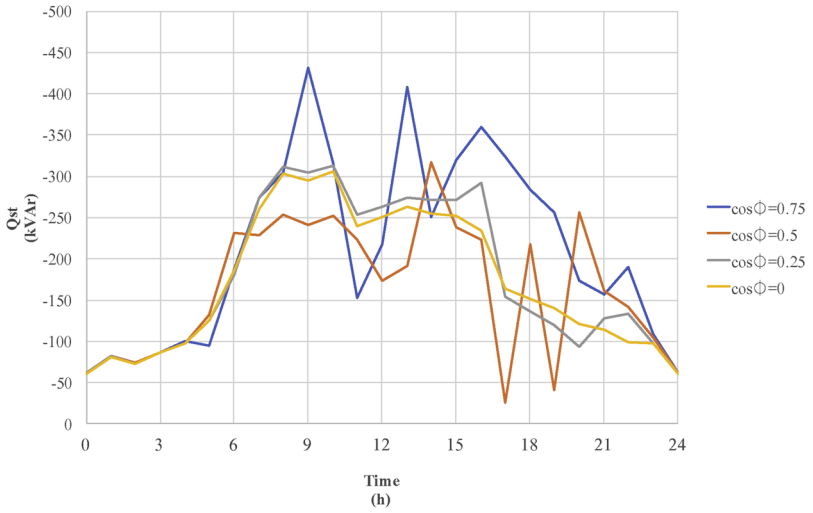

Fig. 19. Reactive power produced by battery inverter connected to busbar 9 of case study A with different power factor limitation.

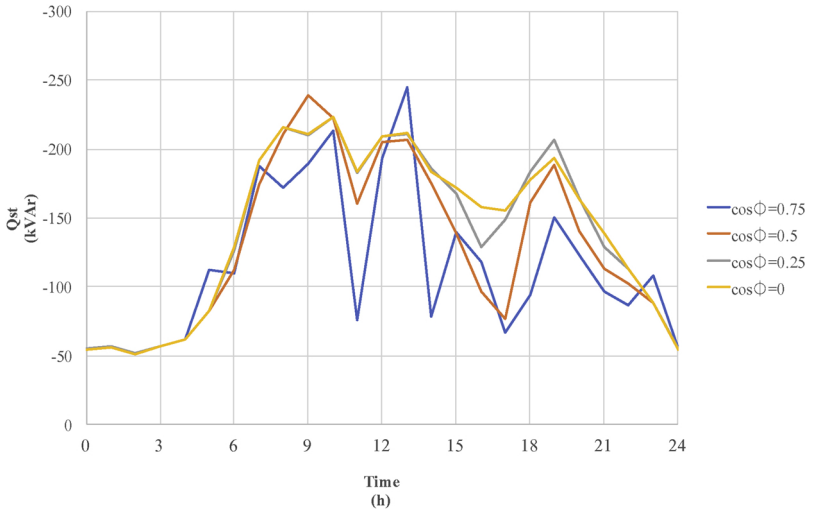

Fig. 20. Reactive power produced by battery inverter connected to busbar 3 of case study A with different power factor limitation.

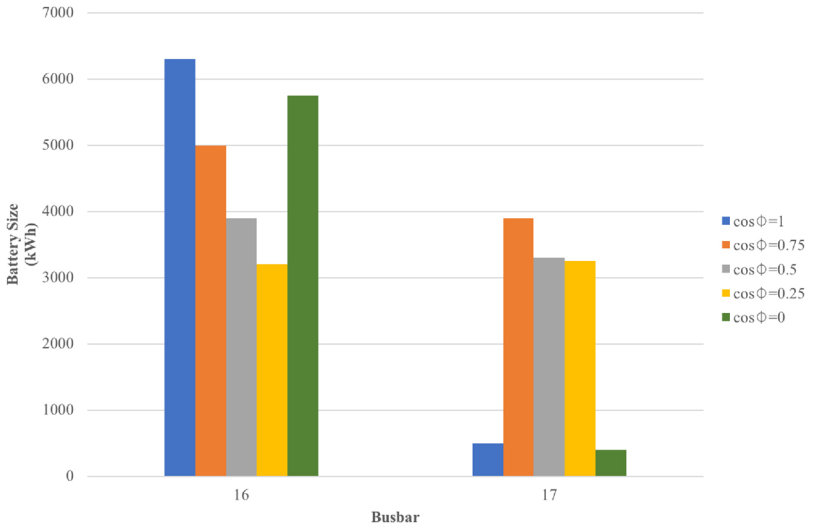

Fig. 21. Batteries size calculated by single loop optimization with different power factor limitation of the battery inverter in case study B.

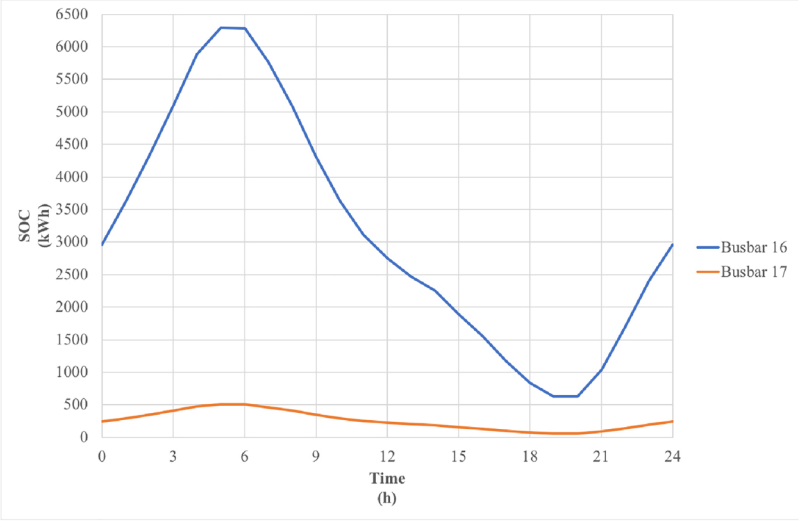

(a)

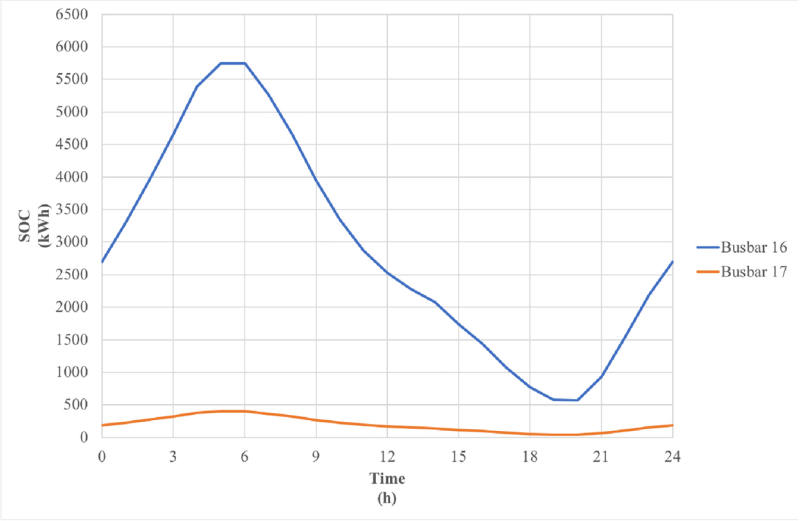

(b)

Fig. 22. State Of Charge for batteries connected to the most sensitive busbars of case study B: (a) storage with $\cos\phi_{lim}=1$; (b) storage with $\cos\phi_{lim}=0$.

residential and industrial load profiles are capable to influence the corresponding line current profiles. Fig. 17 shows instead the line current profile for branch 3 where a mix between residential and industrial load profiles influences the RMS of the branch current.

In all those cases, the placement of storage units on the more sensitive nodes significantly mitigates the branch current variation along the day, reducing the peak demand and making flat the branch current profiles. This effect can be observed both when the reactive power availability is zero (i.e. $\cos\phi_{lim}=1$) and when the battery inverter generates reactive power (i.e. $0 \leq \cos\phi_{lim} < 1$).

However, the operation of the inverter as power factor compensator is more effective, since the local generation covers also the demand of reactive power from the end-users. So, the reactive power generated by battery inverters is strictly correlated to the end-user demand typology where the storage unit is connected. Fig. 18 shows in fact that reactive power generation follows the normalized load profile for residential end-user of Figs. 6 and 7, since only residential load is connected to busbar 6 (see Table A.6. Similarly, Fig. 19 shows how the reactive power generation follows the normalized load profile for industrial end-user, since only industrial load is connected to busbar 9. Finally, Fig. 20 shows a mixed reactive power generation profile, since a mix of industrial and residential users are connected to node 3.

6.2. Case study B

The batteries size obtained for different power factor limitation of battery inverter in the case study B are presented in Fig. 21. As already observed in the previous Section for the case study A, if the power factor is strongly limited (e.g. $\cos\phi_{lim}=0.75$) the storage size is expected to increase in general, if compared to the configuration with $\cos\phi_{lim}=1$, since the production of higher reactive power can be obtained only when higher real one is exchanged to the battery, as can be observed in the capability curve of Fig. 1. Instead, battery inverter without power factor limitation (i.e. $\cos\phi_{lim}=0$) could have a reduced size, since reactive power can be produced even when real one is not exchanged to the battery. In this particular configuration, where the siting of storage units is limited in only two busbars, the BESS in node 16 decreases its capacity when power factor limitation of inverters is limited to 0.75, since a corresponding increase of storage size is observed in busbar 17, as expected. Instead, without power factor

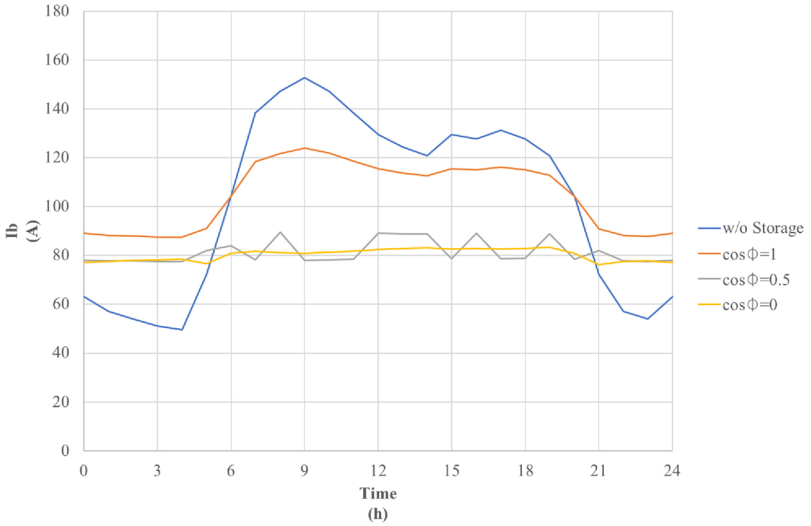

Fig. 23. Line current calculated on branch 14 of case study B with different power factor limitation of the battery inverter.

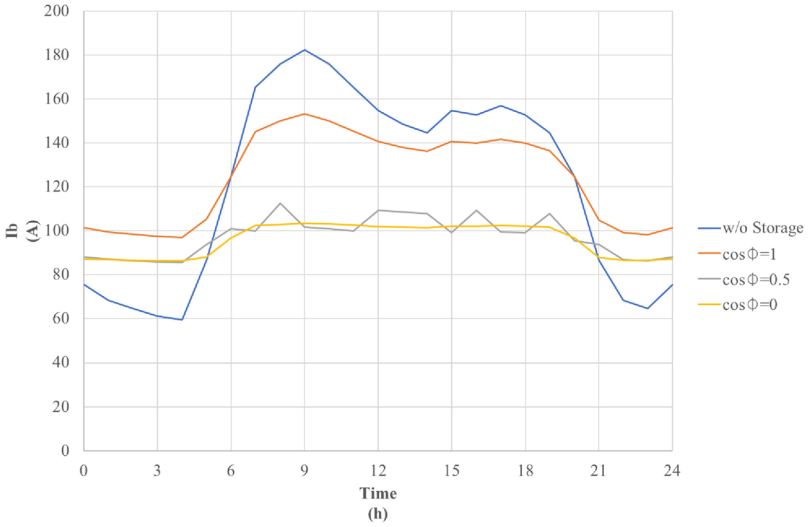

Fig. 24. Line current calculated on branch 12 of case study B with different power factor limitation of the battery inverter.

limitation of the inverter (i.e. $\cos\phi_{lim} = 0$), storage unit increases its capacity in node 16, since a corresponding decrease of storage size is observed in busbar 17, as expected.

The SOC variations due to the management of the battery through the `D-XEMS13` procedure is shown instead in Fig. 22a and b. It is noticeable that the management of the batteries SOC is strongly influenced by the hourly load profile also in this case study B. In fact, since load shifting is expected also in this case study, the BESS stores energy during lower users demand and releases it during period of higher demand. The load profile of Fig. 9, used for describing the end-users connected to the test grid B, shows a substantial higher demand during daytime, but a significant decrease during nighttime. So, the corresponding SOC tends to decrease during daytime and increase during nighttime.

As a consequence of the SOC management, the flattening of the branches current profiles is also reached, since this configuration still represents a minimum for the power losses. Figs. 23 and 24 highlight the trend of the RMS value of the current for branch 12 and 14. The placement of storage units significantly mitigates the branch current variation along the day, reducing the peak demand and making flat the branch current profiles. This effect can be observed both when the reactive power availability is zero (i.e. $\cos\phi_{lim}=1$) and when the battery inverter generates reactive power (i.e. $0 \leq \cos\phi_{lim} < 1$).

It is noticeable that the closer is the siting of the storage unit, more relevant is the flattening effect of the branch current. In fact, the current variation is better compensated by BESS in branch 14 instead of 12, since that branch is closer to the BESS siting in node 16 and 17.

Moreover, the operation of the inverter as power factor compensator is effective, since the local production can partially cover also the demand of reactive power from the end-users. So, the reactive power generated by battery inverters is strictly correlated to the end-user demand typology. Fig. 25 shows in fact that reactive power generation follows the normalized load profile used for the end-users of Fig. 9.

Finally, the bus voltages are also evaluated to monitore the limits imposed by the European standard EN50160 [27] for the test grid of case study B. Differently from the case study A, the topology and the load level of the test grid highlight how the busbars voltage are not compliant to the standard requirement in some cases (i.e. ± 10% of its rated value) when no storage units are connected to the grid. In fact, the maximum voltage drop on busbars reaches around 13.3% of the rated value (i.e. 12.5 kV) as shown in Fig. 26a. Fig. 26b shows that the introduction of batteries without reactive power generation reduces the voltage drops down to 12.2%, but the compliancy to the standard is not reached yet. Finally, Fig. 26c shows instead that the introduction of batteries with production of reactive power by battery inverter, further reduce the voltage drops in busbars. In particular, when battery

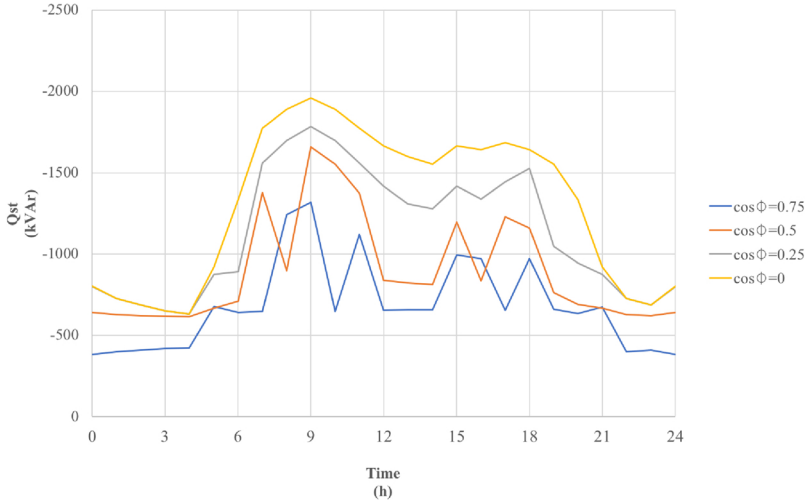

Fig. 25. Reactive power produced by battery inverter connected to busbar 16 of case study B with different power factor limitation.

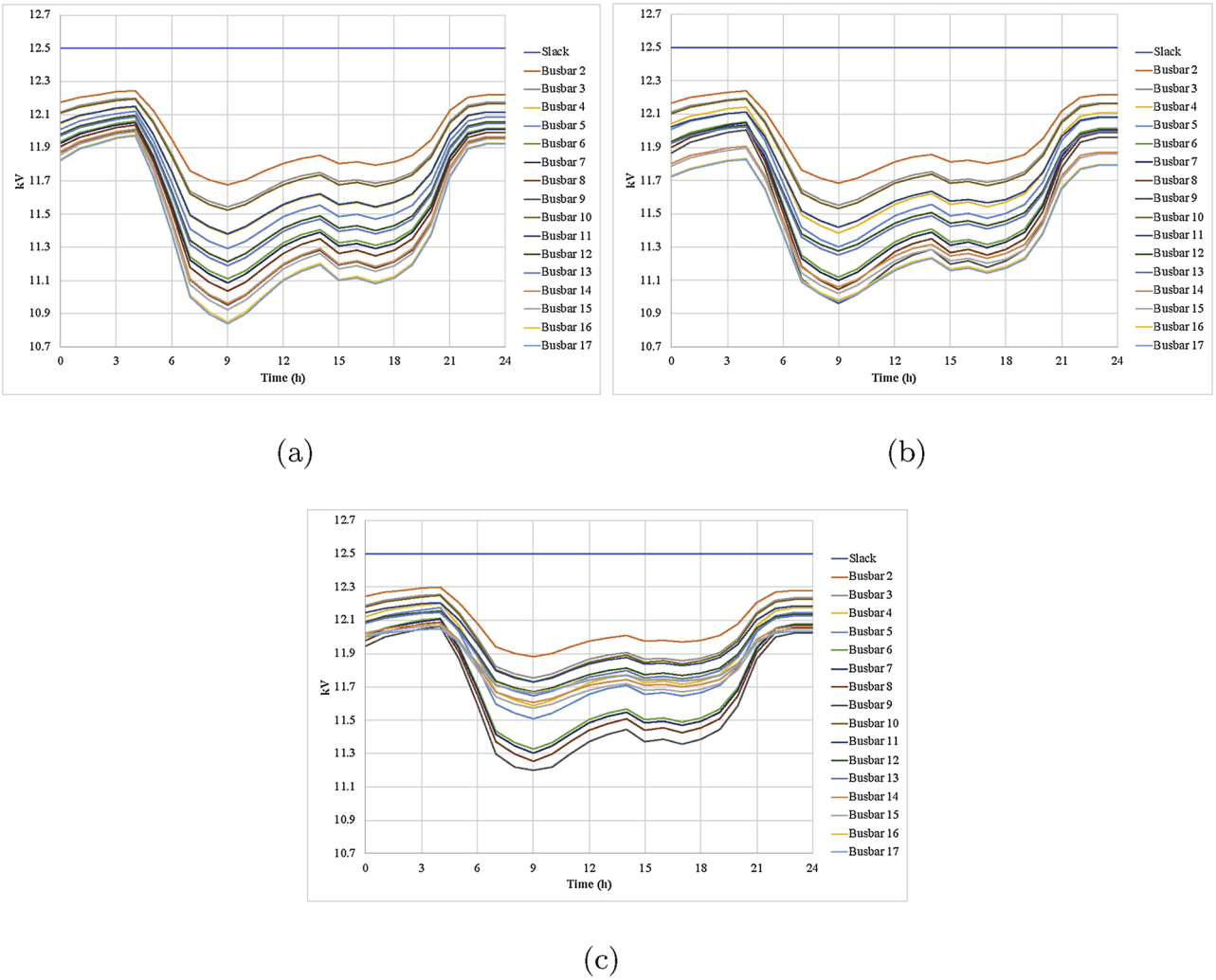

Fig. 26. Busbar voltage profiles of case study B: (a) w/o storage; (b) storage with $\cos\phi_{lim}=1$; (c) storage with $\cos\phi_{lim}=0$.

inverter has no power factor limitation (i.e. $\cos\phi_{lim}=0$) the voltage drop is limited to 9.98% ensuring the compliancy to the standard. As a consequence, the placement of storage units significantly contributes to reduce voltage drops along branches ensuring compliance to the European standard.

7. Conclusion

This paper presents a MIQCQP formulation called `D-XEMS13` integrated within a Backward/Forward Sweep Method to evaluate and minimize network power losses by the introduction of battery energy

storage system in radial distribution grid. The formulation allows to find the optimal management of the battery energy content taking into account its technical characteristics and the possible limitation due to the capability curve of the battery inverter. The D-XEMS13 optimization procedure was subsequently integrated within a single loop optimization algorithm based on direct search method (Pattern Search) where optimal size of battery units can be also evaluated. Results were pointed out by the implementation of the optimization procedure in two different case study of radial test grid without RES generation.

Firstly, the single loop optimization was used to validate a proposed sensitivity analysis in order to identify the best siting of the storage units which ensures the maximum reduction of network power losses according to a reduced size of storage units. The proposed approach was validated by the progressive introduction of battery unit up to connect a storage unit in all the busbars. The evaluation of the ratio between power losses reduction and overall storage size in each configuration highlights and confirms that only a reduced number of nodes are sensitive from power losses point of view. So, the BESSs were placed only in busbars with relevant sensitivity according to the result of the performed analysis.

Secondly, once the best location of battery was validated and identified, a further application of the single loop algorithm on the test grid evaluates and highlights the impacts of the capability curve for the battery inverter in the BESS sizing and power losses reduction. The results highlight the relevance of the reactive power generation which contributes to the reduction of the storages size needed to minimize the network power losses. Hence, also economic benefits can be potentially gained, since reduction of battery investment costs could be obtained. However, the main results reveal further advantages. In particular, the flattening of the branch currents (i.e. load leveling) strongly reduces peaks and it consequently contributes to reduce overcurrent or congestion issues for the DSO during the management of the grid operation. Moreover, the voltage drops reduction ensure compliance to the European standards required for MV distribution grid.

As a general remark, the simulations of the case studies pointed out that the convergence of the iterative Backward/Forward Sweep Method is strictly correlated to the grid topology, its characteristics and the loading level. Thus, in case of lightly loaded and short distribution network with low voltage drops, the convergence is quickly reached. Vice versa, highly loaded and wide radial distribution feeders with corresponding higher voltage drops can lead to increased computational time for reaching the convergence.

More specifically, the proposed approach is limited to radial DN, so further development for considering also weakly meshed DN will be performed in future through, for example, a compensation-based power flow method. Moreover, future investigations will be also performed considering production from RES and DG and BESS installation costs, because of the generality of the proposed approach.

Finally, results of the simulations refer to test grid from literature, so a further application of the optimization procedure in real radial system will be also performed. This could lead to an increased complexity of the problem in terms of computational time due both to the introduction of a growing number of hourly load profiles which can differ, even significantly, from node to node and to the increase of the number of control variables of the problems when large networks are studied. However, not significant difference of the general results highlighted in this paper are expected, because again of the generality of the proposed approach.

Appendix A. Data of case study

Tables A.4–A.8

Table A.4
Transformer data used in the case study A.

Node from	Node to	V_1 [kV]	V_2 [kV]	Z_{tr} [p.u.]	S_n [MVA]	I_m [p.u.]	P_{Fe} [kW]
0	1	110	20	0.001 + j0.12	25	0	0
0	12	110	20	0.001 + j0.12	25	0	0

Table A.5
Lines data of the case study A.

Node from	Node to	Length [km]	R [Ω]	X [Ω]	Installation
1	2	2.82	0.7529	0.5732	Underground
2	3	4.42	1.1801	0.8984	Underground
3	4	0.61	0.1629	0.1240	Underground
4	5	0.56	0.1495	0.1138	Underground
5	6	1.54	0.4112	0.3130	Underground
6	7	0.24	0.0641	0.0488	Underground
7	8	1.67	0.4459	0.3395	Underground
8	9	0.32	0.0854	0.0650	Underground
9	10	0.77	0.2056	0.1565	Underground
10	11	0.33	0.0881	0.0671	Underground
11	4	0.49	0.1308	0.0996	Underground
3	8	1.30	0.3471	0.2642	Underground
12	13	4.89	2.2240	1.7914	Overhead
13	14	2.99	1.3599	1.0953	Overhead
14	8	2.00	0.9096	0.7327	Overhead

Table A.6
Load data used in the case study A.

Busbar	Peak apparent power [kVA]		Power factor (ind.)	
	Residential	Industrial	Residential	Industrial
1	15300	5100	0.98	0.95
2	-	-	-	-
3	285	265	0.97	0.85
4	445	-	0.97	-
5	750	-	0.97	-
6	565	-	0.97	-
7	-	90	-	0.85
8	605	-	0.97	-
9	-	675	-	0.85
10	490	80	0.97	0.85
11	340	-	0.97	-
12	15300	5280	0.98	0.95
13	-	40	-	0.85
14	215	390	0.97	0.85

Table A.7
Lines data of the case study B.

Node from	Node to	R [Ω]	X [Ω]
1	2	0.00312	0.06753
2	3	0.00431	0.01204
3	4	0.00601	0.01677
4	5	0.00316	0.00882
5	6	0.00896	0.02502
6	7	0.00295	0.00824
7	8	0.01720	0.02120
8	9	0.04070	0.03053
3	10	0.01706	0.02209
2	11	0.02910	0.03768
11	12	0.02222	0.02877
12	13	0.04803	0.06218
12	14	0.03985	0.05160
14	15	0.02910	0.03768
14	16	0.03727	0.04593
16	17	0.02208	0.02720

Table A.8
Load data used in the case study B.

Busbar	**Real power [kW]**	**Reactive power [kVAr]**	**Power factor (ind.)**
1	-	-	-
2	-	-	-
3	200	120	0.86
4	400	250	0.85
5	1500	930	0.85
6	3000	2260	0.80
7	800	500	0.85
8	200	120	0.86
9	1000	620	0.85
10	500	310	0.85
11	1000	620	0.85
12	300	190	0.84
13	200	120	0.86
14	800	500	0.85
15	500	310	0.85
16	1000	620	0.85
17	200	120	0.86

References

[1] Treatment of Losses by Network Operators - Ergeg Position Paper. European Regulators' Group for Electricity and Gas, 2008 Technical report.
[2] E. Pons, M. Repetto, A topological reconfiguration procedure for maximising local consumption of renewable energy in (italian) active distribution networks, Int. J. Sustain. Energy 36 (9) (2016) 887–900.
[3] Z. Qing, Y. Nanhua, Z. Xiaoping, Y. You, D. Liu, Optimal siting and sizing of battery energy storage system in active distribution network, 4th IEEE/PES Innovative Smart Grid Technologies Europe (ISGT EUROPE) (2013).
[4] S.B. Karanki, D. Xu, B. Venkatesh, B.N. Singh, Optimal location of battery energy storage systems in power distribution network for integrating renewable energy sources, IEEE Energy Conversion Congress and Exposition (ECCE) (2013).
[5] I. Staffella, M. Rustomjib, Maximising the value of electricity storage, Journal of Energy Storage 8 (2016) 212–225.

[6] Battery storage for renewables: Market status and technology outlook, International Renewable Energy Agency (IRENA), 2015 Technical report.
[7] Commission Staff Working Document. Energy storage - the role of electricity, European Commission, 2017 Technical report,.
[8] N.S. Pearre, L.G. Swan, Technoeconomic feasibility of grid storage: mapping electrical services and energy storage technologies, Appl. Energy 137 (2015) 501–510.
[9] Guido Carpinelli, Gianni Celli, Susanna Mocci, Fabio Mottola, Fabrizio Pilo, Daniela Proto, Optimal integration of distributed energy storage devices in smart grids, Trans. Smart Grid 4 (2) (2013) 985–995.
[10] Matija Zidar, Pavlos S. Georgilakis, Nikos D. Hatziargyriou, Tomislav Capuder, Davor Škrlec, Review of energy storage allocation in power distribution networks: applications, methods and future research, IET Generation Transmission Distribution 10 (3) (2015) 645–652.
[11] Yichen Zhang, Alexander Melin, Mohammed Olama, Seddik Djouadi, Jin Dong, Kevin Tomsovic, Battery energy storage scheduling for optimal load variance minimization, IEEE PES Innovative Smart Grid Technologies Conference (2018).
[12] M. Nazif Faqiry, Lawryn Edmonds, Haifeng Zhang, Amin Khodaei, Hongyu Wu, Transactive-market-based operation of distributed electrical energy storage with grid constraints, Energies 10 (1891) (2017).
[13] Leonardo H. Macedo, John F. Franco, Marcos J. Rider, Rubén Romero, Optimal operation of distribution networks considering energy storage devices, IEEE Trans. Smart Grid 6 (6) (2015) 2825–2836.
[14] John F. Franco, Marcos J. Rider, Rubén Romero, A mixed-integer quadratically-constrained programming model for the distribution system expansion planning, Electr. Power Energy Syst. 62 (2014) 265–272.
[15] Mostafa Nick, Rachid Cherkaoui, Mario Paolone, Optimal allocation of dispersed energy storage systems in active distribution networks for energy balance and grid support, Trans. Power Syst. 29 (5) (2014) 2300–2310.
[16] E. Bompard, E. Carpaneto, G. Chicco, R. Napoli, Convergence of the backward/forward sweep method for the load flow analysis of radial distribution systems, Electr. Power Energy Syst. 22 (7) (2000) 521–530.
[17] Paolo Lazzeroni, Sergio Olivero, Federico Stirano, Maurizio Repetto, Battery energy storage system usage in a distribution grid for PV exploitation: a middle-east case study, IECON 2016-42nd Annual Conference of the IEEE Industrial Electronics Society (2016) 1998–2003.
[18] G. Celli, E. Ghiani, M. Loddo, F. Pilo, An heuristic technique for the optimal planning of meshed mv distribution network, IEEE Russia Power Tech (2005).
[19] Luigi Debarberis, Paolo Lazzeroni, Sergio Olivero, Vito A. Ricci, Federico Stirano, Maurizio Repetto, Technical and economical evaluation of a PV plant with energy storage, IECON 2013-39th Annual Conference of the IEEE Industrial Electronics (2013).
[20] Pierre Bonami, Mustafa Kilinç, Jeff Linderoth, Mixed Integer Nonlinear Programming, Springer, 2012.
[21] http://www.neplan.ch.
[22] Singiresu S. Rao, Engineering Optimization Theory and Practice, Wiley, 2009.
[23] CIGRÉ Task Force C6.04.02, Benchmark systems for network integration of renewable and distributed energy resources, (2009).
[24] M. Farrokhifar, S. Grillo, E. Tironi, Loss minimization in medium voltage distribution grids by optimal management of energy storage devices, IEEE Grenoble PowerTech (POWERTECH) (2013).
[25] T.M. Letcher, Storing Energy with Special Reference to Renewable Energy Sources, Elsevier, 2016.
[26] http://www.gurobi.com.
[27] EN50160 Standard Voltage Characteristics of Electricity Supplied by Public Distribution Systems.